16. Lyadskiy P. V., Chen-Len-Son B. I., Kvasnyuk L. N., Alekseeva G. A., Olenitsa T. V. et al. State geological map of the Russian Federation. Scale 1:200 000. 2nd Edition. Series South Ural. Sheet M-41-VII(XIII) (Svetly). Explanatory note. Moscow MF FGBU VSEGEI, 2018. 128 p.

17. Kolomoets A. V., Snachev A. V., Rassomakhin M. A. Gold–tourmaline mineralization in carbonaceous shales of the Kumak deposit (South Ural). *Gornyi Zhurnal*. 2020. No. 12. pp. 11–15.

18. Snachev A. V., Kolomoets A. V., Rassomakhin M. A., Snachev V. I. Geology and gold content of carbonaceous shale in Baikal mineralization site, Southern Ural. *Eurasian Mining*. 2021. No. 1. pp. 8–13.

19. Yudovich Ya. E., Ketris M. P. Geochemistry of black shales. Moscow. Berlin: Direct Media, 2015. 272 p.

20. Nesbitt H. W., Young G. M. Early Proterozoic climates and plate motions inferred from major element chemistry of lutites. *Nature*. 1982. Vol. 299. pp. 715–717.

21. Herron M. M. Geochemical classification of terrigenous sands and shales from core or log data. *Journal of Sedimentary Petrology*. 1988. Vol. 58. pp. 820–829.

22. Cullers R. L. Implications of elemental concentrations for provenance, redox conditions, and metamorphic studies of shales and limestones near Pueblo, CO, USA. *Chemical Geology*. 2002. Vol. 191, No. 4. pp. 305–327.

23. Roser B. P., Korsch R. J. Provenance signatures of sandstone–mudstone suites determined using discriminant function analysis of major-element data. *Chemical Geology*. 1988. Vol. 67, Iss. 1–2. pp. 119–139.

24. Jones B., Manning D. Comparison of geochemical indices used for the interpretation of paleoredox conditions in ancient mudstones. *Chemical Geology*. 1994. Vol. 111, Iss. 1–4. pp. 111–129.

25. Kholodov V. N., Naumov R. I. On the geochemical criteria for the appearance of hydrogen sulfide contamination in the waters of ancient reservoirs. *Proceedings of the Academy of Sciences of the USSR. Geology series*. 1991. Vol. 12. pp. 74–82.

26. Taylor S. R., Mc Lennan S. M. The Continental Crust: Its Composition and Evolution. Blackwell : Oxford, UK, 1985. 312 p.

27. Wakita H., Rey P., Schmitt R. A. Abundances of the 14 rare-earth elements and 12 other trace elements in Apollo 12 samples: fife igneous and one breccia rocks and four soils. *Proceedings of the 2nd Lunar Science Conference*. Oxford : Pergamon Press. 1971. pp. 1319–1329.

28. Cherepanov A. A., Berdnikov N. V., Shtareva A. V. Rare-earth elements and noble metals in phosphorites of the Gremuchy Occurrence, Lesser Khingan, Far East of Russia. *Russian Journal of Pacific Geology*. 2019. Vol. 13, No. 6. pp. 585–593.

29. Cherepanov A. A., Berdnikov N. V., Shtareva A. V., Krutikova V. O. Formation conditions and rare-earth mineralization of Riphean Carbonaceous shales of the Upper Nyatygran subformation, Russian Far East. *Russian Journal of Pacific Geology*. 2017. Vol. 11, No. 4. pp. 297–307.

30. Paikaray S., Banerjee S., Mukherji S. Geochemistry of shales from the Paleoproterozoic to Neoproterozoic Vindhyan Supergroup: Implications on provenance, tectonics and paleoweathering. *Journal of Asian Earth Sciences*. 2008. Vol. 32, Iss. 1. pp. 34–48.

31. Palenova E. E., Rozhkova E. A., Belogub E. V., Rassomakhin M. A. MREE minerals in black shales of the Paleoproterozoic Mikhailovka formation (Baikal-Patom highland, Siberia). *Mineralogy*. 2022. Vol. 8, No. 3. pp. 47–66.

32. Zanin Yu. N., Zamirailova A. G., Eder V. G., Krasavchikov V. O. Rare-earth elements in the Bazhenov formation of the West-Siberian sedimentary basin. *Lithosphere*. 2011. No. 6. pp. 38–54.

33. Warr L. IMA–CNMNC approved mineral symbols. *Mineralogical Magazine*. 2021. Vol. 85, Iss. 3. pp. 291–320.

34. Kovalev S. G., Maslov A. V., Kovalev S. S. Mineralogical and geochemical aspects of rare-earth elements behavior during metamorphism (on the example of the Upper Precambrian structural-material complexes of the Bashkir megaanticlinorium, South Urals). *Georesources*. 2020. Vol. 22, No. 2. pp. 56–66. EM

M. A. E. IBRAHIM[1], Post-Graduate Student, mohammedelsharif7@gmail.com
A. E. KOTELNIKOV[1], Associate Professor, Head of Department, Candidate of Geological and Mineralogical Sciences
A. F. GEORGIEVSKIY[1], Associate Professor, Doctor of Geological and Mineralogical Sciences
S. A. IBRAHIM[2], Head of Department, Candidate of Geological and Mineralogical Sciences

[1]Peoples' Friendship University of Russia (RUDN University), Moscow, Russia
[2]University of Khartoum, Khartoum, Sudan

GEOCHEMISTRY AND PETROGENESIS OF SYROSTAN GRANITOID INTRUSIONS IN THE SOUTHERN URALS

Introduction

Granite intrusions are often associated with different minerals (for example, ores W, Sn, Nb, Ta, Li, Be, Rb, Cs and REE) [1, 2]. There are some known ore runs within the Syrostan Massif, including skarn bodies and gold-bearing quartz veins. Understanding of distribution of elements in the course of their evolution from magma to hydrothermal phase indispensably requires a profound knowledge on petrogenesis and tectonic mechanism of granite intrusions.

This study aims to reveal petrological features of the Syrostan granite to improve understanding of its formation conditions and mineralization potential.

The article characterizes geochemistry and petrogenesis of granitoids of the Syrostan Massif located southwest of the town of Miass, in the zone of the main deep fault in the Urals. The geochemistry of the collected samples from Syrostan was analyzed using ICP-MS and the X-ray fluorescence. Granite is rich in silicon oxide SiO_2 at its concentrations from 59.54 to 76.14 wt.%. The rocks are from metaluminous to peraluminous and belong to the high-K calc-alkaline to weakly calc-alkaline series; granite is type I and has A/CNK < 1. The test samples feature the higher content of LREE as compared with HREE, the ratios (La / Sm)N from 3.5 to 6.5 and (Gd /Yb)N from 1.25 to 2.8, and the negative Eu anomaly. The revealed negative Nb anomalies and the ratio Nb/Ta (8– 16) <17 point at depletion of mantle melts. These results can be reflective of the granite formation in the tectonic environment of the volcanic arc. Understanding of the petrogenesis of granitoids in the Syrostan Massif can help predict commercial accumulations of rare metals in it.

Keywords: Syrostan Massif, geochemistry, high alkaline granites, type I granite, continental crust, depleted mantle, volcanic arc, ICP-MS
DOI: 10.17580/em.2023.02.02

Regional geology and tectonics

The Syrostan Massif occurs southwestward of Miass town, in the zone of the main Ural deep fault (**Fig. 1**), among metabasites and shales of various compositions as well as fragments of metamorphic oceanic crust and passive margin crust of the Ural paleo ocean [3, 4]. The Massif has a polyphase structure established during the Lower Carbon. The first phase represents grandiorite and quartz diorite, the second phase is plagiogranite and the third phase is a dyke system [5, 6].

The Massif represents an isometric body (see fig. 1). Its root zone in the south is opened up with surface mines. This zone is composed of migmatitic gabbroids and anatectic grandiorites. The center and the north of the Massif are mostly composed of biotite granite and grandiorite. In the southwest, there are local adamellite and granite with small lenticular gabbro bodies [7, 8].

Analytical methods and samples

Rock samples for the petrographic and geochemical analyses were collected during the on-site research. After thorough examination of numerous microsections under a microscope (Altami), nine samples were selected for the geochemical analysis: microgranite (3 samples), leucogranite (3 samples), biotite granite (2 samples) and one sample of diorite. X-ray fluorescence spectroscope (XRF) was used to determine concentrations of petrogenic oxides and some microelements. At the Institute of Mineralogy, Geochemistry and Crystal Chemistry of Rare Elements, Russia, using the inductively coupled plasma mass spectrometry (ICP-MS), the contents of microadmixtures and REE were measured in four samples.

Results
Petrographic research

Microgranites contain quartz (15–25%), microcline (20–50%), plagioclase (20–40%) and biotite (5–10%), and have a medium-grain or coarse-grain structure (**Fig. 2a**). In plagioclase, sericite, muscovite and epidote develop. In zonal plagioclase, the contents of epidote and sericite grow from the core to the periphery (**Fig. 2b**).

Quartz (15–20%), plagioclase (35–55%), microcline (15–35%) and biotite (5–15%) make the most part of biotite granite. The accessory minerals are apatite and monazite (**Fig. 2c**). Leucogranites contain up to 30–35% of quartz, 20–30% of plagioclase, 10–15% of potassic feldspar and from 0 to 5%p of biotite. Biotite often contains noddles of zircon. Diorites contain plagioclase (50–55%), biotite (15–35%) (**Fig. 2d**), potassic feldspar (5–10%), quartz (5–10%) and amphibole (0–5%).

Geochemical features and classification of granitoid rocks

The Total Alkaline Silica (TAS) and modal classifications classify granitoid rocks as mostly granite and diorite (syenodiorite) [9] (**Fig. 3a**). Granite is rich in silicon dioxide SiO_2 at concentrations from 59.54 to 76.14 wt.%. Diorite has an intermediate chemical composition (SiO_2 — 52.89 wt.%). Granitoids feature high total alkalines $K_2O + Na_2O$ (7–10 wt.%), moderate ratio K_2O/Na_2O (0.37–0.83) and a very low or average content of CaO (0.5–6 wt.%) at extremely low values of P_2O_5 (0.01–0.5%). The loss on ignition (LOI) is also mostly low and ranges from
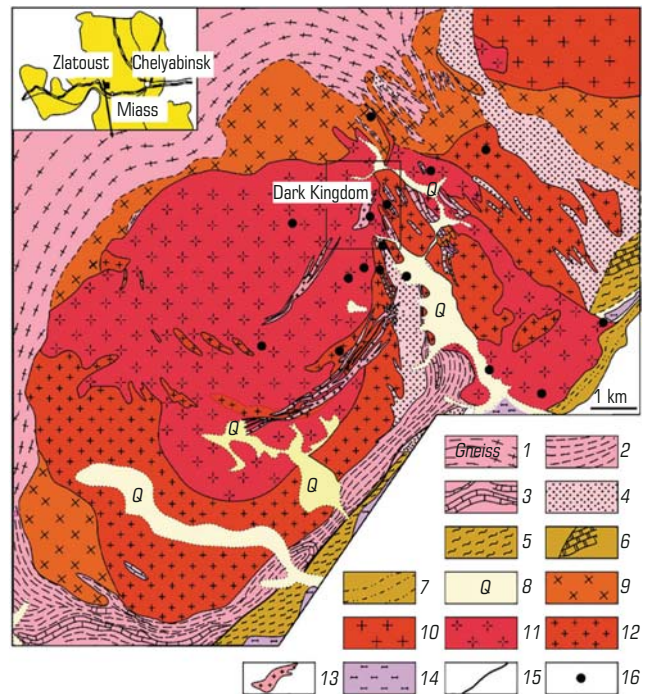

Fig. 1. Geological map of the Syrostan Granite Massif enclosing the Dark Kingdom Marble Deposit ([2] as amended)
Legend: *1* — gneiss; *2* — micaceous quartz shale; *3* — marmorized limestone; *4* — quartzite; *5* — shale; *6* — marble; *7* — carbonaceous shale; *8* — quaternary deposits; *9* — grandiorite, quartz diorite, diorite; *10* — porphyry biotite granite; *11* — pink porphyry biotite granite; *12* — fine-grained granite and plagiogranite; *13* — pegmatite; *14* — serpentine; *15* — tectonic faults; *16* — niobium occurrences
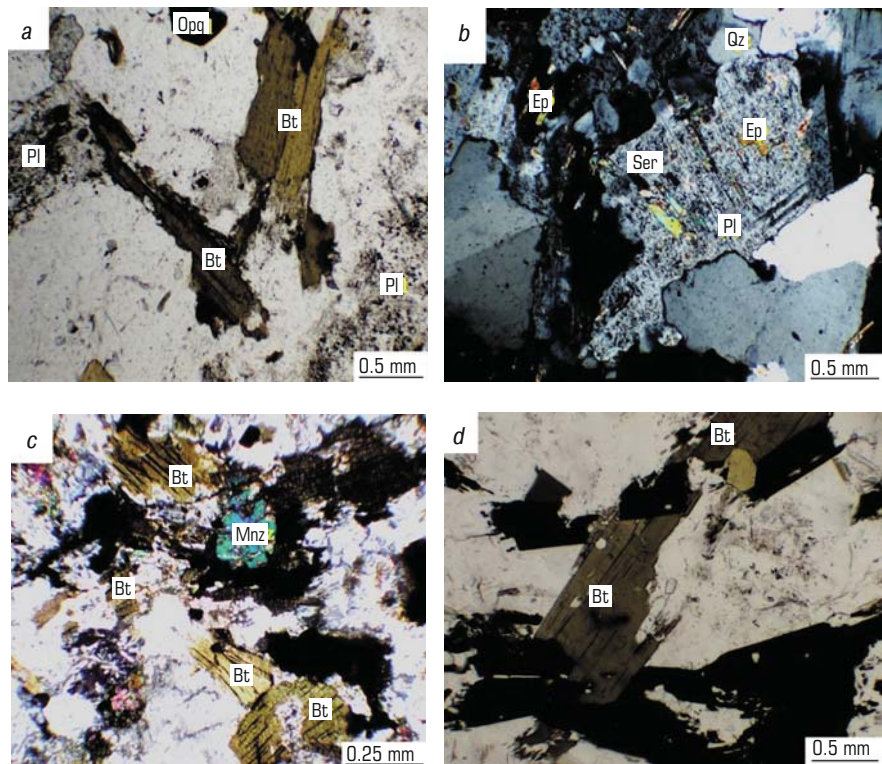

Fig. 2. Microimages of granites and diorites
a — granite composed of quartz, plagioclase and biotite (without analyzer analysis); *b* — plagioclase grains partly replaced by sericite aggregate (with analyzer analysis); *c* — revealed monazite (with analyzer analysis); *d* — revealed biotite in diorite (without analyzer analysis)
Mineral symbols: Opq — opaque minerals; Qz — quartz; Pl — plagioclase; Mc — microcline; Bt — biotite; Ep — epidote; Ser — sericite; Mnz — monazite
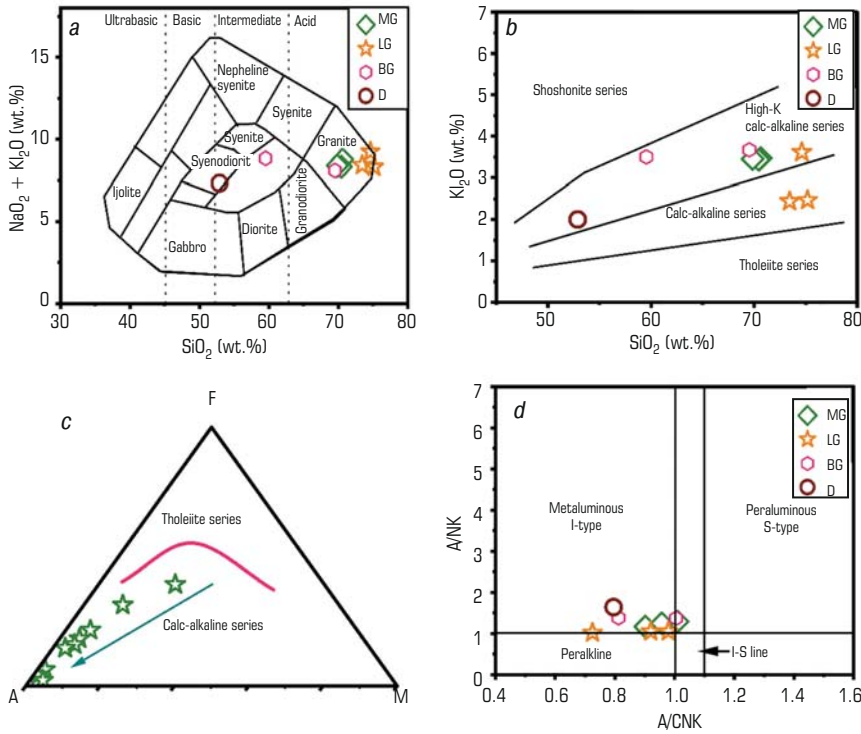
Strontium content of Syrostan Massif rocks

Strontium content	Rock			
	Microgranite	Leucogranite	Biotite granite	Diorite
ppm	720	180	760	1300

Fig. 3. Classification diagrams for the Miass Massif granitoids

Miass granitoid samples in the diagrams: *a* – (k$_2$O + + Na$_2$O)-SiO$_2$ [9]; *b* – SiO$_2$-K$_2$O [10]; *c* – ACM (A = (k$_2$O + Na$_2$O), F = FeOt, M = MgO) [11]; *d* – A/NK [Al$_2$O$_3$/(Na$_2$O + K$_2$O)] - A/CNK [Al$_2$O$_3$/(CaO + + Na$_2$O + K$_2$O)]

Symbols: MG – microgranite; LG – leucogranite; BG – biotite granite; D – diorite
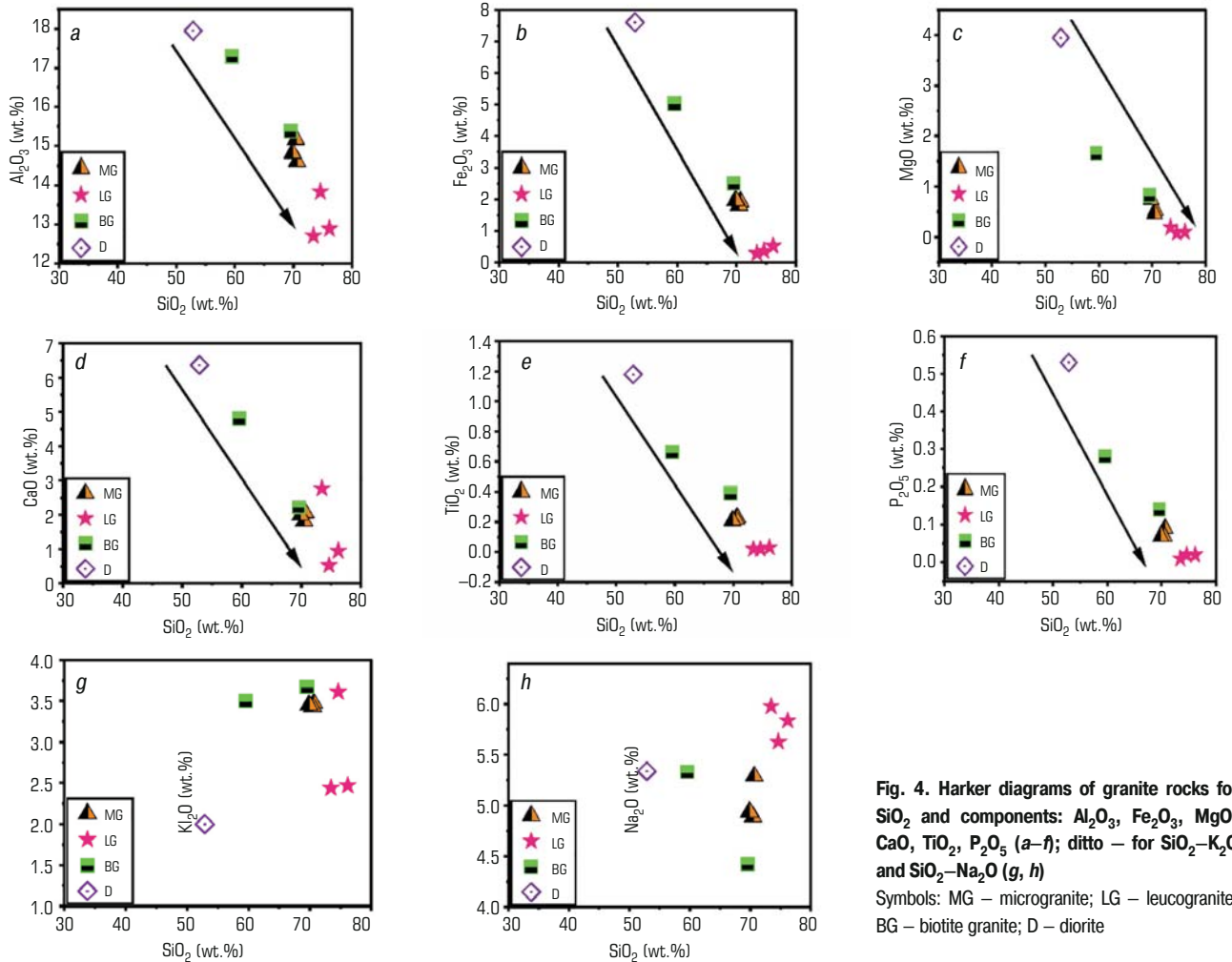
Fig. 4. Harker diagrams of granite rocks for SiO$_2$ and components: Al$_2$O$_3$, Fe$_2$O$_3$, MgO, CaO, TiO$_2$, P$_2$O$_5$ (*a–f*); ditto – for SiO$_2$–K$_2$O and SiO$_2$–Na$_2$O (*g, h*)

Symbols: MG – microgranite; LG – leucogranite; BG – biotite granite; D – diorite

0.6 to 2 wt.%. It follows from the K_2O–SiO_2 diagram [10] that the bulk of the rocks belong to high-K calc–alkaline series and calc–alkaline series (**Fig. 3b**). The same statement follows from the analysis of the ACM diagram [11] (**Fig. 3c**). Furthermore, in the diagram of the Silica Saturation Index (**Fig. 3d**) most granitoids occur in the domain of metaluminous formation, but some samples gravitate toward the domain of peraluminous rocks (see fig. 3d). The supportive data from the analysis of the Harker diagrams describe the behavior of basic oxides (Al_2O_3, Fe_2O_3, MgO, CaO, TiO_2 and P_2O_5) as function of the content of SiO_2 (**Fig. 4**). It is seen from the presented diagrams that the increase of the silica acidity in the test rocks lead to a general decrease in the listed components at their negative correlation with SiO_2 (see fig. 4 a–f). At the same time, the picture is cardinally different in terms of alkalis (K_2O and Na_2O), but it is clear that they have no any correlation with silicon oxide.

Microelements and tectonics

The content of strontium in granitoids of the Syrostan Massif is given in **Table**.

The concentrations of Rb in rocks fluctuate from 10 to 20 ppm, Zr — from 20 to 100 ppm and Hf — from 1.1 to 2.5 ppm. In the tectonic discrimination diagrams (Y + Nb vs Rb, Y vs Nb, Ta + Yb vs Rb), the test samples occur in the field of the volcanic arc granites (VAG) [12] (**Fig. 5a–c**). The same samples in the Yb–Ta diagram are classified as the syncollision–arc granites (syn-COLG) (**Fig. 5d**), while in the Hf–Rb/30–3Ta, they are in the domain of the late- and post-collision granites [13] (**Fig. 5e**). Furthermore, the ratios of the elements detected in the samples are: Rb/Ba (0.05–0.70); Rb/Sr (0.1–0.05); Nb/Ta (8–16); Nb/La (0.6–0.3); Nb/Ce (0.4–0.2); Th/Ta (3.5–8.5) and Zr/Hf (38–52).

The features of rare earths in the test samples are described in **Fig. 6**. As is seen in the spider diagram in Fig. 6a, the rocks are richer in the light rather than heavy REE, at the ratios (La/Sm)N ranged from 3.5 to 6.5 and (Gd/Yb)N from 1.25 to 2.8. The samples have a weak negative europium anomaly (Eu/Eu* 0.2–0.4) with its minimum in leucogranite [Eu (Eu/Eu* 0.18)]. According to fig. 6b, the compositions of granitoids normalized with respect to the mantle components have negative anomalies of Cs, Nb, Pr, Zr, Ti and, partly, Ba and Ce, which may be inherited from the initial magma [15].

Petrogenesis and classification of rocks

Granites of calc–alkaline and high-K calc–alkaline series are known in the Middle and Southern Urals, and are standard type I granites, which is confirmed by the values of the index A/CNK [16, 17]. The indexes A/CNK ([Al_2O_3/($CaO+Na_2O+K_2O$)]) and A/NK (A/NK — [Al_2O_3/(Na_2O+K_2O)]), intrinsic to type I granites, are given in the studies on granitoid masses in the southeast of Asia [18, 19]. The similar values of the indexes in the range of 0.73–1.01 are determined in the Syrostan Massif rocks (see fig. 3d) which belong to the metaluminous and peraluminous varieties [20, 21].

As was noticed, against background of the high total alkalinity (7–10%), the content of P_2O_5 in the Syrostan granites is low (0.01–0.28%) (see fig. 4f). According to [22, 23], this also points at belonging of these rocks to type I granites.

One more interesting feature of the Syrostan granites [22, 23] is the negative correlation between the earlier discussed maphic rock-forming oxides and SiO_2, while Na_2O and K_2O clearly tend to a nonlinear scatter and are weakly correlated with that component. Evidently, this specifics of the rock chemistry should be considered as a sign of crystallization fractionation of magma in the course of its evolution [24, 25]. The crystallization differentiation of the melt magma is also pointed at by the other chemical and mineral components of granitoids [26-28]. In this regard, the most informative sign is the negative anomaly Eu^{2+} <1 identified in leucogranite rocks (see fig. 6a). It is assumed that this fact is reflective of the element removal from the magma composition either owing to protolyte substance concentration in plagioclase minerals or owing to their crystallization from the magma melt during its transformation [29–31].

Tectonics–granitoids correlation

In Pierce's tectonic discrimination diagram (see fig. 5a), the test samples take the field of VAG, which allows supposing formation of the Syrostan Massif in the geodynamic environment of a developing volcanic arc. The similar examples are described in the works [32, 33]. However, as distinct from the described cases, in the Hf–Rb/30–3Ta discrimination diagram [13] (see fig. 5e), the test granite samples occur within the fields of the post-collision and within-the-plate continental environments, which, on the whole, agrees with the high-K and calc–alkaline characteristics of the test granites. This
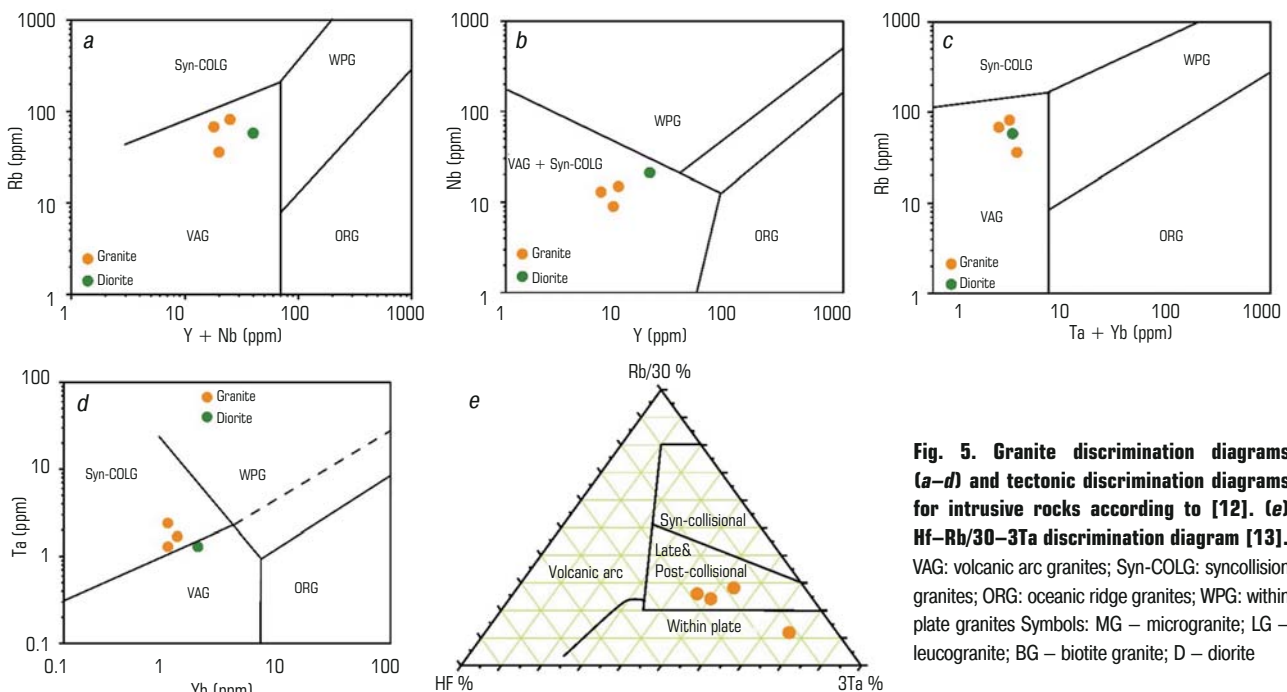

Fig. 5. Granite discrimination diagrams (a–d) and tectonic discrimination diagrams for intrusive rocks according to [12]. (e) Hf–Rb/30–3Ta discrimination diagram [13]. VAG: volcanic arc granites; Syn-COLG: syncollision granites; ORG: oceanic ridge granites; WPG: within plate granites Symbols: MG — microgranite; LG — leucogranite; BG — biotite granite; D — diorite
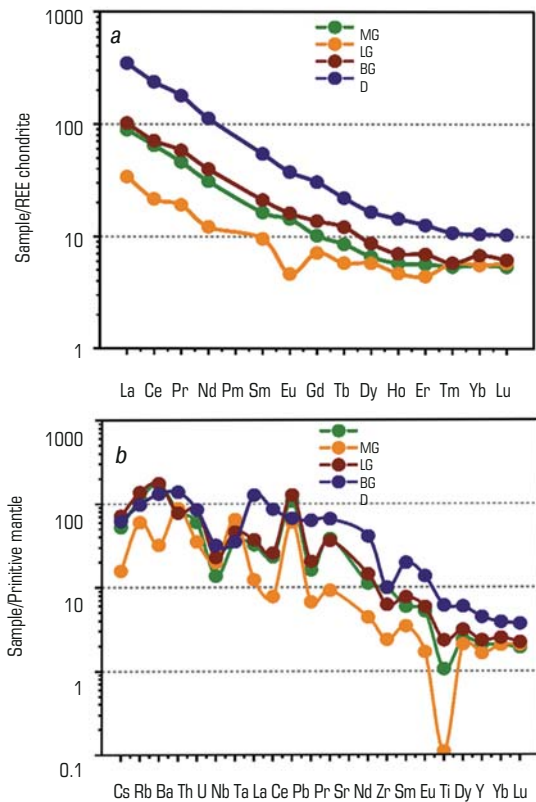
Fig. 6. Spider diagram (*a*) of rare earths distribution in Miass granitoids (REE compositions are normalized with respect to chondrite [14]); (*b*) diagrams of compositions of micro impurities in the same rocks after normalization with respect to primitive mantle [15]

fact can be explained as follows. It is assumed that the volcanic arc magmas form from the LIL rich mantle wedge above the subduction zones in the oceanic lithosphere [34, 35]. Such magmas have geochemical characteristics which are partly preserved in the collision-altered rocks. It is highly probable in this case that compositions of the magma melts were subjected to contamination connected with assimilation of enclosing rocks and, first of all, rocks from the crust bottom. This situation is quite valid for the Syrostan granitoids and is described for some regions in [36–38]. The proof of this statement is the compositions of the Syrostan granites normalized with respect to primitive mantle (see fig. 6*b*) [39]. The pronounced negative anomalies of Nb in the figure confirm the participation of the continental crust in the magmatic processes [40–42]. The ratios Nb/Ta (8–16) < 17 point at the existence of melts of the depleted mantle, which also follows from the behavior of P and Ti relative to the primitive mantle composition (see fig. 6*b*) [43, 44].

Finally, the above-discussed data allow assuming formation of granitoids of the Syrostan Massif in the geodynamic mode of the volcanic arc given crystallization of the magma melts formed during partial melting of the continental substance in the zone of slab subduction [45, 46].

Conclusions

Granitoids of the Syrostan Massif are rich in silicon oxide SiO_2 at concentrations from 59.54 to 76.14 wt.%. Diorites have an intermediate content of SiO_2 at 52.89 wt.%. The test samples are characterized with the high values of the summed alkaline $K_2O+Na_2O = (7–9$ wt.%) and ratios K_2O/Na_2O in the range from 0.37 to 0.83. The concentrations of P_2O_5 (0.01–0.5%) and CaO (0.5–6%) are low.

The higher contents of the light REE as against the heavy REE are revealed, at the ratios (La/Sm)N from 3.5 to 6.5 and (Gd/Yb)N from 1.25 to 2.8, and at the negative Eu anomaly.

The metaluminous to peraluminous rock belong to high-K to weakly calc-alkaline series. The basic geochemical characteristics allow classifying the test granitoids as type I granites.

It is highly probable that the Syrostan Massif was formed under the island-arc geodynamic mode under the conditions of partial melting of the over-slab continental substance.

References

1. Xie L., Liu Y., Wang R., Hu H., Che X. et al. Li–Nb–Ta mineralization in the Jurassic Yifeng granite-aplite intrusion within the Neoproterozoic Jiuling batholith, south China: A fluid-rich and quenching ore-forming process. *Journal of Asian Earth Sciences.* 2019. Vol. 185. DOI: 10.1016/j.jseaes. 2019.104047

2. Makagonov E. P., Muftahov V. A. Rare-earth and rare-metal mineralization in late granite of Syrostan massif (Southern Urals). *Lithosfere.* 2015. No. 2. pp. 121–132.

3. Fershtater G. B., Paleozoic Intrusive Magmatism of the Middle and South Urals. Yekaterinburg : UB RAS, 2013. 368 p.

4. Makaganov E. P., Muftahov V. A. Rare metals of the Syrostan Massif granitoids, South Urals, *South Ural State University's Science — The 67th Conference Proceedings.* Chelyabinsl : Izdatelskyi centr YuURGU, 2015. pp. 430–437.

5. Georgievskiy A. F., Bugina V. M., Kotelnikov A. E., Georgievskiy A. A., Mahinja E. et al. Vein-rock in the Dark kingdom Marble Deposit (South Ural) and their Possible Connection with Gold Ore Mineralization. *International Science and Technology Conference on Earth Sciences–2020.* Vladivostok : IOP Publishing Ltd, 2021. DOI: 10.1088/1755-1315/666/2/022024.

6. Bea F., Fershtater G. B., Montero P., Smirnov V. N., Molina J. F. Deformation-driven differentiation of granitic magma: The Stepninsk pluton of the Uralides, Russia. *Lithos.* 2005. Vol. 81, No. 1–4. pp. 209–233.

7. Montero P., Bea F., Gerdes A., Fershtater G., Zinkova E. et al. Single-zircon evaporation ages and Rb-Sr dating of four major Variscan batholiths of the Urals A perspective on the timing of deformation and granite generation. *Tectonophysics.* 2000. Vol. 317, No. 1–2. pp. 93–108.

8. Udoratina O. V., Kulikova K. V., Shuyskiy A. S., Soboleva A. A., Andreichev V. L. et al. Granitoid magmatism in the North of the Urals: U–Pb age, evolution, sources. *Geodynamics & Tectonophysics.* 2021. Vol. 12, No. 2. pp. 287–309.

9. Cox K. G., Bell J. D., Pankhurst R. J. The interpretation of igneous rocks. George, Allen and Unwin, London, Boston, Sydney, 1979.

10. Peccerillo A., Taylor S. R. Geochemistry of eocene calc-alkaline volcanic rocks from the Kastamonu area, Northern Turkey. *Contributions to Mineralogy and Petrology.* 1976. Vol. 58, No. 1. pp. 63–81.

11. Irvine T. N., Baragar W. R. A. A Guide to the Chemical Classification of the Common Volcanic Rocks. *Canadian Journal of Earth Sciences.* 1971. Vol. 8, No. 5. pp. 523–548.

12. Pearce J. A., Harris N. B. W., Tindle A. G. Trace element discrimination diagrams for the tectonic interpretation of granitic rocks. *Journal of Petrology.* 1984. Vol. 25, Iss. 4. pp. 956–983.

13. Harris N. B. W., Pearce J. A., Tindle A. G. Geochemical characteristics of collision-zone magmatism. *Geological Society, London, Special Publications.* 1986. Vol. 19, No. pp. 67–81.

14. Anders E., Grevesse N. Abundances of the elements: Meteoritic and solar. *Geochimica et Cosmochimica Acta.* 1989. Vol. 53, No. 1. pp. 197–214.

15. McDonough W. F., Sun S. The composition of the Earth. *Chemical Geology.* 1995. Vol. 120, No. 3-4. pp. 223–253.

16. Korovin D. D. Geochemical features of the Devonian plutonic rocks of the Reftinsky massif (Middle Urals). *News of the Ural State Mining University*. 2022. Vol. 1(65). pp. 13–21.

17. Znamensky S. E. Petrological and geochemical characteristic of the rocks of the voznesensky intrusive massif (Southern Urals): On the question of the composition and sources of magma producing gold and copper porphyry mineralization. *Lithosphere*. 2021. Vol. 21, No. 3. pp. 365–385.

18. Uchida E., Nagano S., Nik S., Yonezu K., Saitoh Y. et al., Geochemical and radiogenic isotopic signatures of granitic rocks in Chanthaburi and Chachoengsao provinces, southeastern Thailand: Implications for origin and evolution. *Journal of Asian Earth Sciences X*. 2022. Vol. 8. DOI:10.1016/j.jaesx.2022.100111

19. Yang Yu, Min Sun, Xiaoping Long, Pengfei Li, Guochun Zhao, et al. Whole-rock Nd–Hf isotopic study of I-type and peraluminous granitic rocks from the Chinese Altai: Constraints on the nature of the lower crust and tectonic setting. *Gondwana Research*. 2017. Vol. 47. pp. 131–141.

20. Wu F. Y., Liu X. C., Ji W. Q., Wang J. M., Yang L. Highly fractionated granites: Recognition and research. *Science China Earth Sciences*. 2017. Vol. 60. pp. 1201–1219.

21. Kuzmin V. K., Naumov M. V., Rodionov N. V., Zelepugin V. N., Yurchenko Y. Y. Paleoproterozoic granitoids in the Luktur Complex, the Yurovsky Uplift (Okhotsk Massif): composition, age and genesis according to geochemical, Nd-Sr isotope-geochemical and U-Pb geochronological data. *Regional Geology and Metallogeny*. 2022. Vol. 90. pp. 58–77.

21. Liu D., Zhao Z., Yan J., Shi Q. The Sangri highly fractionated I-type granites in southern Gangdese: Petrogenesis and dynamic implication. *Acta Petrologica Sinica*. 2017. Vol 33(8). pp. 2479–2493.

22. Chappell B. W., White A. J. R. I- and S-type granites in the Lachlan Fold Belt. *Special Paper of the Geological Society of America*. 1992. Vol. 272. pp. 1–26.

23. Li C., Yan J., Yang C., Song C. Z., Wang A. G. et al. Generation of leucogranites via fractional crystallization: A case study of the Jurassic Bengbu granite in the southeastern North China Craton. *Lithos*. 2020. Vol. 352-353. DOI:10.1016/j.lithos.2019.105271

24. Dio Rizqi Irawan, Endang Wiwik Dyah Hastuti. Karakteristik batuan granitoid formasi granit Garba Daerah Tekana dan sekitarnya, Kabupaten OKU Selatan, Sumatera Selatan. *Journal of Earth and Energy Sriwijaya University*. 2020. Vol. x. pp. 1–12.

25. Eskandari A., Deevsalar R., Rosa R. De, Shinjo R., Donato P. et. al. Geochemical and isotopic constraints on the evolution of magma plumbing system at Damavand Volcano, N Iran. *Lithos*. 2020. Vol. 354-355. DOI:10.1016/j.lithos.2019.105274

26. Przybyło A., Pietranik A., Zieliński G. Cerium and Ytrium in apatite as records of magmatic processes: Insight into fractional crystallization, magma mingling and fluid saturation. *Geochemistry*. 2022. Vol. 82, Iss. 2. DOI:10.1016/j.chemer.2022.125864

27. Naumov V. B., Dorofeeva V. A., Girnis A. V., Kovalenker V. A. Volatile, Trace, and Ore Elements in Magmatic Melts and Natural Fluids: Evidence from Mineral-Hosted Inclusions. II. Effect of Crystallization Differentiation on the Concentrations of Ore Elements. *Geochemistry International*. 2022. Vol. 60, No. 6. pp. 537–550.

28. Scaillet B., France-Lanord C., Le Fort P. Badrinath-Gangotri plutons (Garhwal, India): petrological and geochemical evidence for fractionation processes in a high Himalayan leucogranite. *Journal of Volcanology and Geothermal Research*. 1990. Vol. 44, No. 1-2. pp. 163–188.

29. Lee S. G., Asahara Y., Tanaka T., Lee S. R., Lee T. Geochemical significance of the Rb-Sr, La-Ce and Sm-Nd isotope systems in A-type rocks with REE tetrad patterns and negative Eu and Ce anomalies: The Cretaceous Muamsa and Weolaksan granites, South Korea. *Geochemistry*. 2013. Vol. 73, Iss. 1. pp. 75–88.

30. Shan H., Zhai M., Lu X. Petrogenesis delineation of the felsic intrusive rocks in the eastern North China Craton: Implications for crustal evolution and geodynamic regimes. *Lithos*. 2022. Vol. 422-423. DOI:10.1016/j.lithos.2022.106728

31. Kholodnov V. V., Shardakova G. Yu., Puchkov V. N., Petrov G. A., Shagalov E. S. et al. Paleozoic granitoid magmatism of the urals: the reflection of the stages of the geodynamic and geochemical evolution of a collisional orogen. *Geodynamics & Tectonophysics*. 2021. Vol. 12(2). pp. 225–245.

32. Gillespie M. R., Kendall R. S., Leslie A. G., Millar I. L., Dodd T. J. H. et al. The igneous rocks of Singapore: New insights to Palaeozoic and Mesozoic assembly of the Sukhothai Arc. *Journal of Asian Earth Sciences*. 2019. Vol. 183. DOI:10.1016/j.jseaes.2019.103940

33. Clemens J. D., Darbyshire D. P. F., Flinders J. Sources of post-orogenic calcalkaline magmas: The Arrochar and Garabal Hill-Glen Fyne complexes, Scotland. *Lithos*. 2009. Vol. 112, Iss. 3–4. pp. 524–542.

34. Parnachev V. P. Elementaries of Geodynamic Analysis. Tomsk : NTL, 2014. 316 p.

35. Yarmolyuk V. V., Kuzmin M. I., Vorontsov A. A. West pacific-type convergent boundaries and their role in the formation of the Central Asian fold belt. *Russian Geology and Geophysics*. 2013. Vol. 54, No. 12. pp. 1427–1441.

36. Eyal M., Litvinovsky B., Jahn B. M., Zanvilevich A., Katzir Y. Origin and evolution of post-collisional magmatism: Coeval Neoproterozoic calc-alkaline and alkaline suites of the Sinai Peninsula. *Chemical Geology*. 2010. Vol. 269, Iss. 3-4. pp. 153–179.

37. Ghoneim M. F., Abdel-Karim A. A. M., Abu Anbar M. M., Nageib A., El-Shafei S. A., Petrogenesis of postcollisional high-K calc-alkaline and alkaline magmatism in Southern Sinai, Egypt: The role of crustal anatexis combined with convective diffusion. *The Journal of Geology*. 2022. Vol. 130, No. 2. pp. 111–132.

38. Dong P., Dong G., Santosh M., Mo X., Sun Z., et al. Eocene magmatism in the western Tengchong Block: Implications for crust-mantle interaction associated with the slab rollback of the Neo-Tethys Ocean. *Gondwana Research*. 2022. Vol. 106. pp. 259–280.

39. Zaikova V. V. Metallogeny of ancient and modern oceans. Volcanism and ore formation. Miass : UrO RAN, 2018. 316 p.

40. Gao L., Liu S., Sun G., Hu Y., Guo R. et al. Neoarchean crust-mantle interactions in the Yishui Terrane, south-eastern margin of the North China Craton: Constraints from geochemistry and zircon U-Pb-Hf isotopes of metavolcanic rocks and high-K granitoids. *Gondwana Research*. 2019. Vol. 65. pp. 97–124.

41. Fadaeian M., Jahangiri A., Ao S., Kamali A. A., Xiao W. Geochemistry and petrogenesis of Shoshonitic Dyke Swarm in the Northeast of Meshkinshahr, NW Iran. *Minerals*. 2022. Vol. 12, Iss. 3. pp. 1–27.

42. He X., Tan S., Liu Zh., Bai Zh., Wang X. et al. Petrogenesis of the early cretaceous aolunhua adakitic monzogranite porphyries, Southern Great Xing'an Range, NE China: Implication for geodynamic setting of Mo mineralization. *Minerals*. 2020. Vol. 10, Iss. 4. DOI:10.3390/min10040332

43. Stolz A. J., Jochum K. P., Spettel B., Hofmann A. W. Fluid- and melt-related enrichment in the subarc mantle: Evidence from Nb/Ta variations in island-arc basalts. *Geology*. 1996. Vol. 24, No. 7. pp. 587–590.

44. Meng L.-T., Chen B.-L., Zhao N.-N., Wu Y., Zhang W.-G. et al. The distribution, geochronology and geochemistry of early Paleozoic granitoid plutons in the North Altun orogenic belt, NW China: Implications for the petrogenesis and tectonic evolution. *Lithos*. 2017. Vol. 268–271. pp. 399–417.

45. Kosarev A. M., Seravkin I. B., Kholodnov V. V. Geodynamic, petrological and geochemical aspects of zoning Magnitogorsk pyrite megazone in Southern Ural. *Lithospere*. 2014. No. 2. pp. 3–25.

46. Imamverdiyev N.A. Delamination of subducted lithospheric slab as a reason of late cenozoic collision volcanism in the Lesser Caucasus. Vestnik Bakinskogo Gosudarstvennogo Universiteta. *Seriya estestvennykh nauk*. 2008. No. 3. 𝐄𝐌